



# An approach to localize the retinal blood vessels using bit planes and centerline detection

M.M. Fraz<sup>a,\*</sup>, S.A. Barman<sup>a</sup>, P. Remagnino<sup>a</sup>, A. Hoppe<sup>a</sup>, A. Basit<sup>b</sup>,  
B. Uyyanovara<sup>c</sup>, A.R. Rudnicka<sup>d</sup>, C.G. Owen<sup>d</sup>

<sup>a</sup> Digital Imaging Research Centre, Faculty of Science and Engineering, Kingston University London, London, United Kingdom

<sup>b</sup> TPPD, Pakistan Institute of Nuclear Science and Technology (PINSTECH), Nilore, Islamabad, Pakistan

<sup>c</sup> Department of Information Technology, Sirindhorn International Institute of Technology, Thammasat University, Pathum Thani, Thailand

<sup>d</sup> Division of Population Health Sciences and Education, St. George's, University of London, London, United Kingdom

## ARTICLE INFO

### Article history:

Received 30 March 2011

Received in revised form

25 July 2011

Accepted 29 August 2011

### Keywords:

Medical imaging, Retinal image  
Ocular fundus

Image segmentation

Blood vessel segmentation

First order derivative of Gaussian

Bit plane slicing

Mathematical morphology

## ABSTRACT

The change in morphology, diameter, branching pattern or tortuosity of retinal blood vessels is an important indicator of various clinical disorders of the eye and the body. This paper reports an automated method for segmentation of blood vessels in retinal images. A unique combination of techniques for vessel centerlines detection and morphological bit plane slicing is presented to extract the blood vessel tree from the retinal images. The centerlines are extracted by using the first order derivative of a Gaussian filter in four orientations and then evaluation of derivative signs and average derivative values is performed. Mathematical morphology has emerged as a proficient technique for quantifying the blood vessels in the retina. The shape and orientation map of blood vessels is obtained by applying a multidirectional morphological top-hat operator with a linear structuring element followed by bit plane slicing of the vessel enhanced grayscale image. The centerlines are combined with these maps to obtain the segmented vessel tree. The methodology is tested on three publicly available databases DRIVE, STARE and MESSIDOR. The results demonstrate that the performance of the proposed algorithm is comparable with state of the art techniques in terms of accuracy, sensitivity and specificity.

© 2011 Elsevier Ireland Ltd. All rights reserved.

## 1. Introduction

The morphological features of retinal vessels have been related to cardiovascular risk factors in childhood and adulthood, such as blood pressure and body size [1], and with cardiovascular outcomes in later life, including both coronary heart disease and stroke [2]. Automatic detection and analysis of the retinal vasculature can assist in the implementation

of screening programs for diabetic retinopathy [3], the evaluation of retinopathy of prematurity [4], foveal avascular region detection [5], arteriolar narrowing detection [6], the determination of the relationship between vessel tortuosity and hypertensive retinopathy [7], measurement of vessel diameter to diagnose cardiovascular diseases and hypertension [8], and computer-assisted laser surgery [9]. Automatic generation of retinal maps and extraction of branch points have been used for temporal or multimodal image registration [10],

\* Corresponding author. Tel.: +44 7864567523.

E-mail address: [moazam.fraz@yahoo.com](mailto:moazam.fraz@yahoo.com) (M.M. Fraz).

0169-2607/\$ – see front matter © 2011 Elsevier Ireland Ltd. All rights reserved.

doi:10.1016/j.cmpb.2011.08.009

retinal image mosaic synthesis [11], optic disc identification and fovea localization [12]. The retinal vascular tree is found to be unique for each individual and can be used for biometric identification [13]. The manual measurement of the retinal vasculature is a time consuming process that entails training and the skill of the operator. A viable solution is the use of automated analysis, which is nowadays commonly accepted by the medical community.

Retinal vessels are composed of arteriolar and venules, which appear as elongated branched features emanating from the optic disc within a retinal image. Retinal vessels often have strong light reflexes along their centerline, which is more apparent on arteriolar than venules, and in younger compared to older participants, especially those with hypertension. The vessel cross-sectional intensity profiles approximate to a Gaussian shape, or a mixture of Gaussians in the case where a central vessel reflex is present. The orientation and gray level of a vessel does not change abruptly; they are locally linear and gradually change in intensity along their lengths. The vessels can be expected to be connected and, in the retina, form a binary treelike structure. However, the shape, size and local gray level of blood vessels can vary hugely and some background features may have similar attributes to vessels. Arteriolar-venule crossing and branching can further complicate the profile model. As with the processing of most medical images, signal noise, drift in image intensity and lack of image contrast pose significant challenges to the extraction of blood vessels.

In this work, the skeleton of the blood vessels is obtained by the detection of vessel centerlines and the vessel shape and orientation map is produced by morphological bit planes slicing. The segmented vessel tree is generated by the reconstruction of the vessel centerlines image with the vessel shape and orientation map. There are several methods found in the literature for the detection of vessel centerlines in retinal images [8,14–19]. We employ a filter kernel derived by computing the first order derivative of the original matched filter [20] that was initially proposed for vessel detection. The other key contribution is to demonstrate the application of bit planes for retinal vasculature extraction. Moreover, the unique combination of vessel centerlines with morphological bit planes is presented.

The organization of the paper is as follows. Section 2 presents a comprehensive overview of retinal vessel segmentation algorithms available in the literature. Section 3 illustrates the proposed methodology in detail. Some illustrative experimental results of the algorithm on the images of the DRIVE [21], STARE [22] and MESSIDOR [23] databases are presented in Section 4, and discussed in Section 5.

## 2. Retinal vessel segmentation methodologies

Several methods for detecting retinal blood vessels have been reported in the literature, which can be classified in to techniques based on pattern recognition, matched filtering, morphological processing, vessel tracking, multiscale analysis and model based algorithms. We provide a comprehensive review of these methods.

The popular methodology for vessel extraction built upon pattern recognition methods can be further divided into two categories: supervised methods and unsupervised methods. Supervised methods utilize ground truth data for the classification of vessels based on given features. These methods include neural networks [24], back propagation neural network [25], principal component analysis [26], k-nearest neighbor classifiers [27], ridge based primitives classification [14], Gabor wavelet with supervised classification using a mixture of Gaussian [28], line operators and support vector classification [29], multiscale Gabor filter in combination with principal component analysis [30] and a feature based Ada-Boost classifier [31]. The unsupervised methods work without any prior labeling knowledge. Some of the reported methods are the fuzzy C-Means clustering algorithm [32], Radius based Clustering ALgorithm (RACAL) [33], maximum likelihood estimation of vessel parameters [34], matched filtering along with specially weighted Fuzzy C-Means clustering [35] and local entropy thresholding using a gray level co-occurrence matrix [36].

The matched filtering methodology exploits the piecewise linear approximation, the decrease in vessel diameter along vascular length and the Gaussian like intensity profile of retinal blood vessels and uses a kernel based on a Gaussian or its derivatives to enhance the vessel features in the retinal image. The matched filter (MF) was first proposed by Chaudhuri et al. [20] and later adapted and extended by Hoover et al. [37], Xiaoyi and Mojon [38] and Yao and Chen [39]. Freeman and Adelson [40] proposed steerable filters for vessel segmentation which were further extended by Kochner et al. [41]. Chutatape and co-workers [42] evaluated the suitability amplitude-modified second order Gaussian filter whereas Zhang et al. [43] proposed an extension and generalization of the matched filter with a first-order derivative of Gaussian. Al-Rawi et al. [44] improved Chaudhuri's et al. [20] matched filter by using an exhaustive search optimization procedure. A hybrid model of the matched filter and ant colony algorithm for retinal vessel segmentation was proposed by Cinsdikici and Aydin [45]. A high speed detection of retinal blood vessels using phase congruency and a bank of log-Gabor filters has been proposed by Amin and Yan [46].

Morphological processing for identifying specific shapes has the advantage of speed and noise resistance. Zana and Klein [10,47] combined morphological filters and cross-curvature evaluation to segment vessel-like patterns. Ayala et al. [48] defined an average of fuzzy sets by making use of statistical models. Mendonca and Campilho [15] detected vessel centerlines in combination with multiscale morphological reconstruction to segment the blood vessels. Sun et al. [16] combined morphological multiscale enhancement, the fuzzy filter and the watershed transformation for the extraction of the vascular tree in angiograms.

The algorithms based on the vessel tracking methodology segment a vessel between two points using local information and work at the level of a single vessel rather than the entire vasculature. Liu and Sun [49] presented an approach that extracts extended tracts of the vasculature in X-ray angiograms by an adaptive tracking algorithm. Liang et al. [50] developed an algorithm to find the course of the vessel centerline and measure the diameter and the tortuosity of a single

vessel segment. Chutatape et al. [51] used a tracking strategy with Gaussian and Kalman filters for blood vessel detection in retinal images. Quek and Kirbas [52] used wave propagation and a traceback mechanism for retinal blood vessel segmentation. Ali et al. [53] described an algorithm based on recursively tracking the vessels starting from initial seed-points, using directional templates. A semi-automated method for segmentation of vascular images was proposed by Kelvin et al. [54] which incorporated Frangi's et al. [55] multiscale vesselness filtering into the conventional Livewire framework [56] to efficiently compute optimal medial axes. Delibasis et al. [57] presented an automatic model-based tracing algorithm for vessel segmentation and diameter estimation.

The multiscale approaches for vessel segmentation are based on scale-space analysis. The width of a vessel decreases gradually across its length as it travels radially outward from the optic disc. Therefore the idea behind scale-space representation for vascular extraction is to separate out information related to the blood vessel having varying width. Frangi et al. [55] examined the multiscale second order local structure of an image (Hessian) in the context of developing a vessel enhancement filter. A vesselness measure is obtained on the basis of eigenvalue analysis of the Hessian. Martinez-Perez et al. [58] used edge information and the maximum principal curvature to obtain width, size and orientation of retinal blood vessels. An extension [59] of this scale-space algorithm [58] was demonstrated by exploiting the observation that the intensity of an image is proportional to the amount of blood in the light path corresponding to the particular pixel during image capture. The algorithm [58] was further improved by using the insight segmentation and registration toolkit (ITK) [60]. A parallel implementation [61] of this algorithm based on ITK is capable of achieving accuracy comparable to its serial counterpart while providing processing 8–10 times faster which is advantageous for handling higher resolution images and larger datasets. Wink et al. [62] have developed a method for central axis extraction that finds a minimum cost path using the vector-valued multiscale representation of a feature. Sofka and Stewart [17] presented a likelihood ratio test for vessel centerlines extraction that combines matched filter responses, confidence measures and vessel boundary measures. Vlachos and Dermatas [63] proposed a multi-scale line tracking for vasculature segmentation.

The branch of algorithms which traces its roots from model based approaches can further be categorized in to three groups i.e. vessel profile models, active contour models and geometric models based on level sets. The vessel cross-sectional intensity profiles can be approximated by a Gaussian or its higher order derivatives, a mixture of Gaussians or hermite polynomial profile in cases where the central vessel reflex is present. Vermeer et al. [64] modeled the vessel profile as a Laplacian kernel for segmentation. Mahadevan et al. [65] presented a robust and modular framework for vessel detection in noisy images which is based on the estimation of the log likelihood of vessel parameters in a noisy environment using three models; the Huber's censored likelihood ratio test [66], the ranked ordered test [67] for log likelihood and the robust model selection [68] based on nonlinear least squares fitting. The framework is adaptable to incorporate a variety of vessel profile models including Gaussian, derivatives

of Gaussian and dual Gaussian and various noise models like Gaussian noise and Poisson noise. A multiresolution hermite model was proposed for vascular segmentation by Li et al. [69], which employed a two-dimensional hermite function intensity model in a quad-tree structure over a range of spatial resolutions. Lam and Hong [18] proposed a vessel segmentation algorithm for pathological retinal images based on the divergence of vector fields. The algorithm presented by Lam et al. [70] was based on regularization based multiconcavity modeling and was able to handle both normal and pathological retinas with bright and dark lesions simultaneously. Narasimha-Iyer et al. [71] exploited the structural and functional features of dual-wavelength retinal fundus images recorded at 570 and 600 nm for vessel segmentation and identification as arteries and veins. The cross sectional intensity profile of retinal vessels was estimated by the dual-Gaussian model initially used by Xiaohong et al. [72]. Zhu [73] defined a universal representation of vessel cross-sectional profiles in the Fourier domain, utilizing phase congruency to characterize this representation. A number of authors have investigated the use of active contour models, or snakes, in retinal vascular segmentation. Espona et al. [19] used the classical snake in combination with blood vessel topological properties to extract the vasculature from retinal images. Al-Diri and Hunter [74] introduced Ribbon of Twin, a parametric active contour model, which used two contours coupled by spring models to overcome initialization and localized feature problems; and the "ribbon" method, which couples two snakes with a consistent width parameter. Vessel width measurement was also incorporated by Al-Diri et al. in [75]. A number of retinal vessel segmentation algorithms [76–78] were reported in the literature which utilizes the geometric models and theory of curve evolution of geometric flows. These models are usually implemented using the level-set based numerical algorithm.

### 3. Proposed methodology

The foundation of this work is laid upon the identification of the vessel skeleton by detecting the vessel centerlines and vessel shape and orientation map generation through morphological bitplane slicing, an extension of the work presented in [79]. The first order derivative of Gaussian (FoDoG) filter is applied to the monochromatic representation of a background normalized retinal image with enhanced response in four directions. The candidate pixels for vessel centerlines are detected by evaluation of derivative signs and the average derivative values in the four matched filter response (MFR) images. The vessel centerlines pixels are identified in each directional candidate pixel image by using image statistical measures. The shape and orientation map of retinal vessels is acquired with bit planes slicing of a morphologically vessel enhanced image. The enhanced vessel image is the result of the sum of images obtained by applying the top-hat transformation on a monochromatic representation of the retinal image using a line shape structuring element rotated in eight directions. The detected vessel centerlines are then combined with the shape and orientation map to produce the binary segmented vascular tree. The algorithm is tested on variety

of monochromatic representations of colored retinal images including the green channel of RGB color space, the I component of HIS color space, the luminance channel of NTSC(YIQ) color space and  $L^*$ ,  $A^*$ ,  $B^*$  color space.

There are several methods found in the literature for detection of vessel centerlines in retinal images. Lowell et al. [8] uses a tramline filter for labeling of vessel centerlines. The algorithm presented by Staal et al. [14] is based on an extraction of image ridges, which coincide approximately with vessel centerlines. Mendonca and Campilho [15] extracts the vessel centerlines with Difference of Offset Gaussian filter kernel which is derived by subtracting the binomial kernel from itself at a distance along the cardinal axes and is an approximation of the Gaussian derivative. Sun et al. [16] detects vessel centerlines by employing fuzzy morphological enhancement followed by thresholding and morphological thinning. Sofka and Stewart [17] presents a likelihood ratio test for vessel centerlines extraction that combines matched-filter responses, confidence measures and vessel boundary measures. The normalized gradient vector field for centerline extraction is used by Lam and Hong [18]. Espona et al. [19] extracts the vessel centerlines using Multilevel Set Extrinsic Curvature based on the Structure Tensor (MSEC-ST) [80] which guide the proposed contour model for vessel segmentation. In this work, for the detection of vessel centerlines we employ a filter kernel which is derived by computing the first order derivative of the original matched filter [20] that was initially proposed for vessel detection. The other key contribution is to demonstrate the application of bit planes for retinal vasculature extraction.

### 3.1. Detection of centerlines

#### 3.1.1. The filter

The MF was first proposed in [20] to detect vessels in retinal images. The profile of the filter is designed to match that of a blood vessel, which typically has a Gaussian shape curve. The MF is defined as:

$$f(x, y) = \frac{1}{\sqrt{2\pi}\sigma} \exp\left(-\frac{x^2}{2\sigma^2}\right); \quad \text{for } |x| \leq (t, \sigma), \quad |y| \leq \frac{L}{2} \quad (1)$$

And the first order derivative  $g(x, y)$  of  $f(x, y)$  is defined as:

$$g(x, y) = -\frac{x}{\sqrt{2\pi}\sigma^2} \exp\left(-\frac{x^2}{2\sigma^2}\right); \quad \text{for } |x| \leq (t, \sigma), \quad |y| \leq \frac{L}{2} \quad (2)$$

where,  $\sigma$  represents the scale of filter;  $L$  is the length of the neighborhood along the  $y$ -axis;  $t$  is a constant and is usually set to 3 because more than 99% of the area under the Gaussian curve lies within the range  $[-3\sigma, 3\sigma]$ .

The underlying idea is that when a first order derivative filter is applied orthogonally to the main orientation of the vessel, derivative values with opposite signs are obtained on the vessel cross profile and there will be positive values on one side of the vessel cross section and negative values on the other. The maximum local intensity across the blood vessel cross profile in the retina generally occurs at the vessel center pixels, therefore vessel centerlines are measured as the connected sets of pixels which correspond to intensity maxima computed from the intensity profiles of the vessel cross

sections. For this purpose, the FoDoG kernel is rotated every  $45^\circ$  and convolved with the monochromatic representation of the colored retinal image in horizontal, vertical, diagonal and cross diagonal directions.

#### 3.1.2. Image normalization

There is a gradual intensity variation in the background of retinal images taking place from the periphery of the retina towards the central macular region. The vessels are the retinal structures that are prominent from the background but a more careful investigation of local vessel intensities can reveal noteworthy variations that can negatively interfere in the complete vessel segmentation process. To reduce this influence, three preprocessing techniques for monochromatic representation of the original color image are proposed and analyzed before using the first order derivative of Gaussian for centerline extraction.

The intensity variation in the background of the image is normalized by subtracting an estimate of the background from the original image. The estimate is obtained by applying a filtering operation with a large arithmetic mean kernel. In this work, we use a  $31 \times 31$  pixel size kernel and the filtering operation is decimation. The decimated image from this process is resized to the actual size of original image which is then subtracted from the green channel to obtain a normalized image. The background normalized image is shown in Fig. 1(b). In the second technique, the maximum principal curvature [55] of the retinal image is calculated which is illustrated in Fig. 1(c). In this image the vessels are enhanced and background variation is normalized. Moreover, the line detector presented in [29] is utilized to generate the line strength image shown in Fig. 1(d), which is taken as input for the application of FoDoG. The experimental results demonstrate that the later two preprocessing techniques perform slightly better in centerline detection than the first one, but the gain in performance is negligible with an increase in the computational cost. Therefore, in this work we use the arithmetic mean kernel for background intensity normalization.

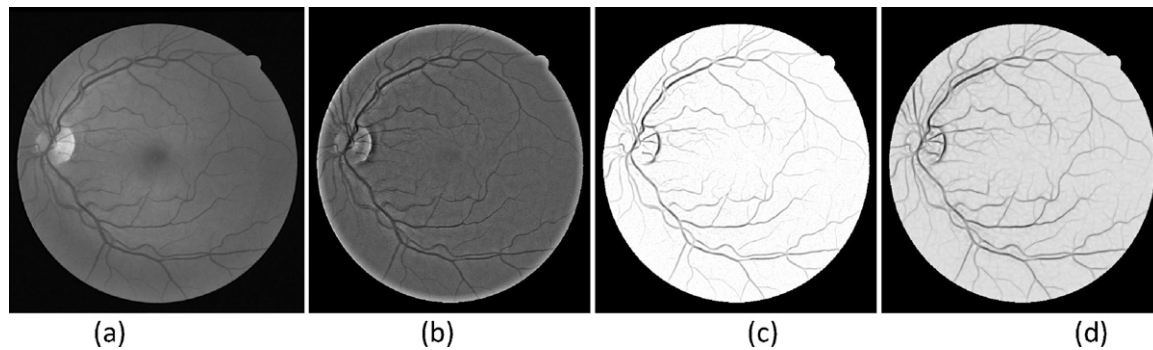
#### 3.1.3. Centerline extraction

The FODOG filter kernel is convolved with the input retinal image in four orientations of  $0^\circ$ ,  $45^\circ$ ,  $90^\circ$  and  $135^\circ$ . The candidate pixels for vessel centerlines are marked by looking for a specific combination of derivative signs across the vessel cross section and orthogonally to the vessel in each one of the resulting four directional images. The detailed procedure of evaluation of derivative sign and average derivative values is available in [15]. The result of this processing sequence is a set of connected segments in one particular direction and the final vessel centerline image is obtained by combining all the four images as shown in Fig. 2.

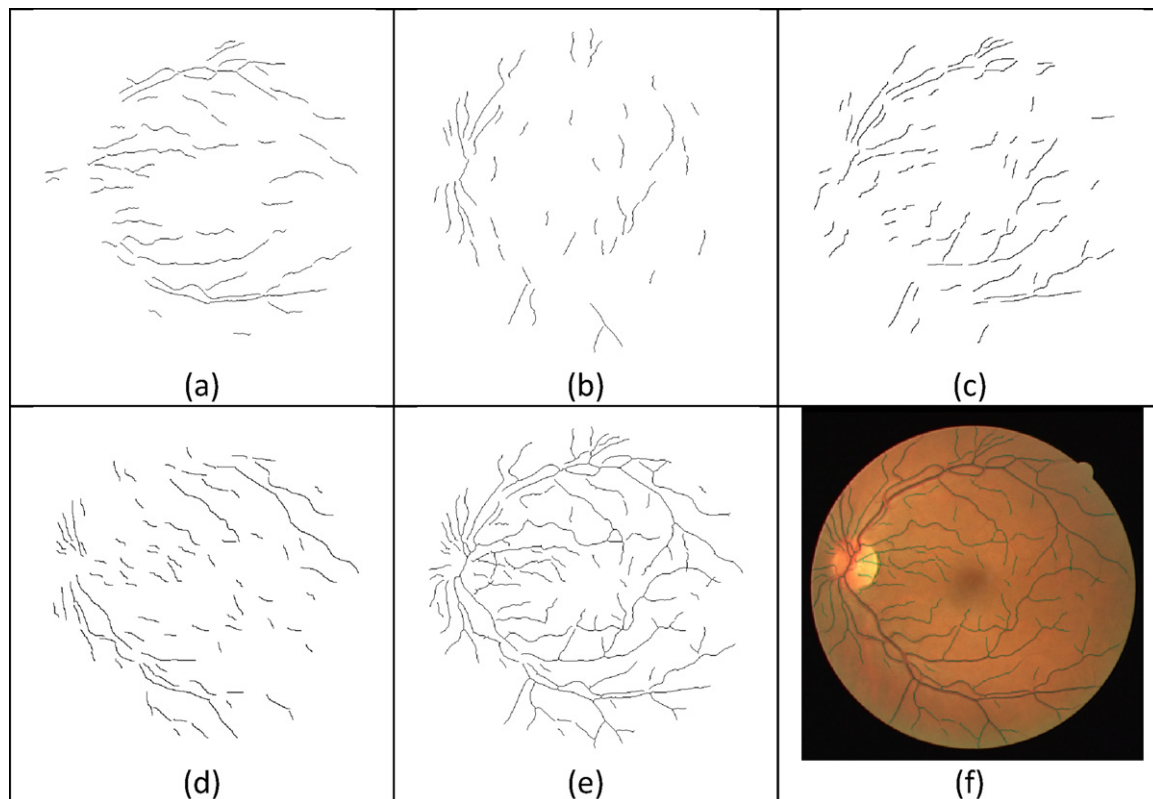
### 3.2. Morphological bit planes slicing

The structure of blood vessels is enhanced in contrast from the background of the retinal image by the application of morphological operators with directional structuring elements and then the significant information of the vessel structure is extracted from bit planes of a grayscale image in order to generate the shape and orientation map of the blood vessels. The





**Fig. 1 – Preprocessed images (a) green channel of RGB image, (b) background normalized, (c) maximum principal curvature (inverted) and (d) line strength image.**



**Fig. 2 – Vessel centerlines: (a–d) Directional vessels centerlines in horizontal, vertical, 45°, 135°, respectively. (e) Vessels centerline image, (f) centerlines superimposed on RGB image.**

segmented vascular tree is obtained by the reconstruction of vessel centerlines with the generated map of blood vessels.

### 3.2.1. Vessel enhancement

Mathematical morphology is a nonlinear tool in image analysis which has revealed itself as a very useful technique for quantifying retinal pathology in fluorescent angiograms and monochromatic retinal images. The basic morphological operations of opening, closing, erosion and dilation of a digital image with a structuring element are defined in [81].

The morphological opening operator, which is actually erosion followed by dilation, acts as a shape filter erasing objects from the image which are smaller in size than

the used structuring element, thus approximating the background. Therefore enhancement of objects which are erased by the opening operation would be achieved by subtracting the opened image from the original image. Without loss of generalization, the assumption is that a vessel is a bright pattern with a Gaussian shape cross section profile on the dark background, and is piecewise connected and linear. Because of the piecewise linear nature of vessels, morphological filters with linear structuring elements are used to enhance the vessels in the retinal image.

Morphological opening using a linear structuring element oriented at a particular angle will eradicate a vessel or part of it when the structuring element cannot be contained within the

vessel. This happens when the vessel and the structuring element have orthogonal directions and the structuring element is longer than the vessel width. Conversely, when the orientation of the structuring element is parallel with the vessel, the vessel will stay nearly unchanged.

$$I_{th}^{\theta} = I - (I \circ S_e^{\theta}) \quad (4a)$$

$$I_{s_{th}} = \sum_{\theta \in A} I_{th}^{\theta} \quad (4b)$$

The morphological top-hat transformation is shown in Eq. (4a) where  $I_{th}^{\theta}$  is the top-hat transformed image,  $I$  is the image to be processed and  $S_e$  is structuring elements for morphological opening  $\circ$  and  $\theta$  is the angular rotation of the structuring element. If the opening along a class of linear structuring elements is considered, a sum of top-hat along each direction will brighten the vessels regardless of their direction, provided that the length of the structuring elements is large enough to extract the vessel with the largest diameter. Therefore, a set of line structuring elements where each one is a matrix representing a line with 21 pixels of length and rotated at every  $22.5^{\circ}$  is used for the morphological top hat transformation. Its size is approximately the range of the diameter of the biggest vessels for retinal images. The sum of the top-hat is depicted in Eq. (4b), where  $I_{s_{th}}$  is the sum of top-hat transformation performed with the structuring element oriented at  $\theta$  degrees. The set  $A$  can be defined as  $\{x | 0 \leq x \leq 180 \text{ and } x \bmod(22.5) = 0\}$ . In the image, every isolated round and bright zone whose diameter is less than the length of the linear structuring element pixels has been removed. The sum of top-hat on the filtered image will enhance all vessels whatever their direction, including small or tortuous vessels as depicted in Fig. 3(b).

### 3.2.2. Bit plane slicing

Bit plane slicing highlights the contribution made to the total image appearance by specific bits. Separating a digital image into its bit planes is useful for analyzing the relative importance played by each bit of the image. It is a process that aids in determining the adequacy of the number of bits used to quantize each pixel.

The image resulting from the sum of the top-hat operation is a monochromatic grayscale in which the gray levels are distributed in such a way that the blood vessels are highlighted more than the background. This 8-bit gray scale image can be represented in the form of bit planes, ranging from bit plane 1 for the least significant bit to bit plane 8 for the most significant bit. It is observed that the higher order bits, especially the top two, contain the majority of the visually significant data. Fig. 4 shows bit plane 7 and bit plane 8 of the vessel enhanced image. The other bit planes contribute to more subtle details in the image and appear as noise. A single binary image is obtained by taking the sum of the top two bit planes which are bit plane 7 and bit plane 8, as shown in Fig. 4(c). This binary image is the approximation of the shape and orientation map of the retinal blood vessels.

### 3.2.3. Vessel tree generation

The final image of the vascular tree is obtained by a reconstruction of the vessel centerlines image and vessel shape and

orientation image. The vessel centerline image is used as seed points and the vessel shape and orientation map as an aggregated image for a simple region growing procedure. The seed pixels of vessel centerlines are compared with neighboring pixels in the map image for 8-connectivity. The region is grown by aggregating the centerlines with the neighboring pixels of the map image satisfying the condition of 8-connectivity. The aggregate threshold for region growing is set to be 1 because of the binary image format. When the augmentation of a selected seed pixel stops, another seed pixel from the vessel centerline image which is not yet aggregated as the vessel region is selected for the region growth. The final vessel segmentation, as shown in Fig. 5(a), is obtained after a cleaning operation aimed at removing all pixels completely surrounded by vessel points but not labeled as part of a vessel. This is done by considering that each pixel with at least six neighbors classified as vessel points must also belong to a vessel.

## 4. Results

In this section, we present the materials on which the retinal vessel segmentation algorithms are evaluated, the performance measures used to evaluate the algorithm, and the obtained results.

### 4.1. Materials

The methodology has been evaluated quantitatively and qualitatively using two established publicly available databases (DRIVE and STARE) and a new public database (MESSIDOR).

The DRIVE[21] database contains 40 color images of the retina, captured by a Canon CR5 3CCD camera with a 45 degree field of view (FOV), with  $565 \times 584$  pixels and 8 bits per color channel. The image set is divided into a test and training set and each one contains 20 images. The performance of the vessel segmentation algorithms is measured on the test set. The test set has four images with pathologies. For the 20 images of the test set, there are two manual segmentations available made by two different observers resulting in a set A and B. The manually segmented images in set A by the 1st human observer are used as a ground truth. The human observer performance is measured using the manual segmentations by the 2nd human observer from set B. In set A, 12.7% of pixels were marked as vessel against 12.3% in set B.

The STARE[22] database contains 20 colored retinal images, with  $700 \times 605$  pixels and 8 bits per RGB channel, captured by a TopCon TRV-50 fundus camera at 35 degree FOV. Two manual segmentations by A. Hoover and V. Kouznetsova are available. The first observer marked 10.4% of pixels as vessel, the second one 14.9%. The performance is computed with the segmentations of the 1st observer as a ground truth. The comparison of the 2nd human observer with the ground truth images gives a detection performance measure which is regarded as a target performance level.

The MESSIDOR [23] database has been established to facilitate studies on computer-assisted diagnoses of diabetic retinopathy. It contains 1200 eye fundus color images which are acquired by a Topcon TRC NW6 non-mydratic retinograph with a  $45^{\circ}$  field of view. The images were captured using 8 bits

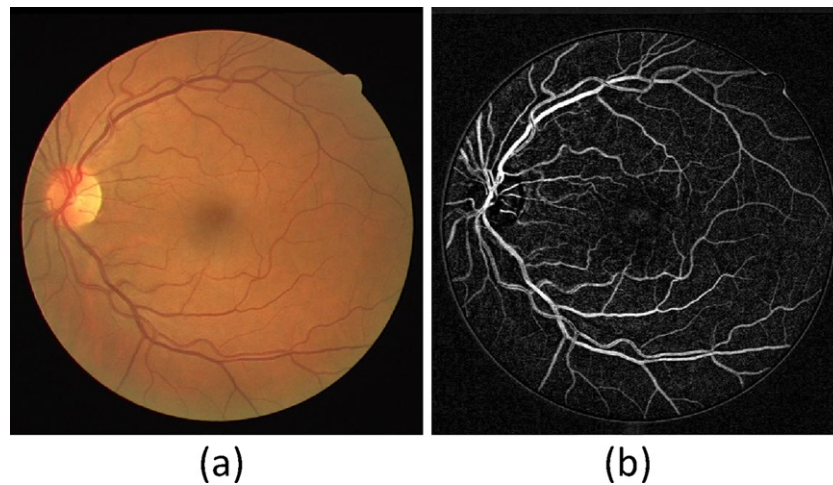


Fig. 3 – Sum of top-hat. (a) Colored retinal image. (b) Image resulted from sum of top-hat transformation.

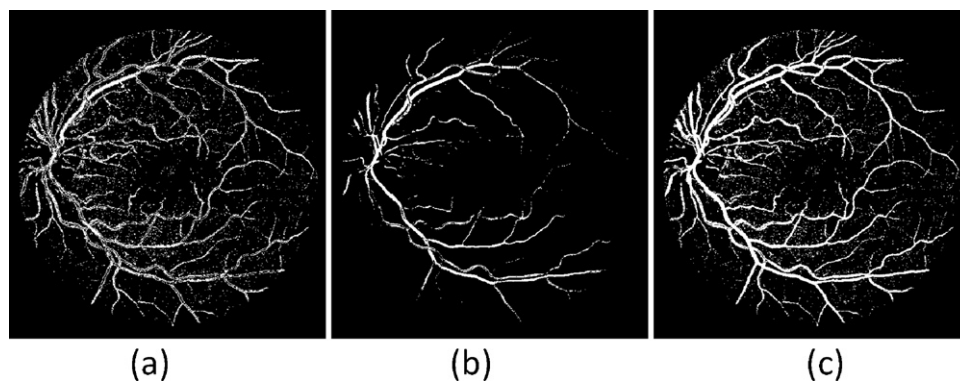


Fig. 4 – Bit planes of the image (a) Bit plane 7, (b) Bit plane 8 and (c) combined bit plane 7 and bit plane 8.

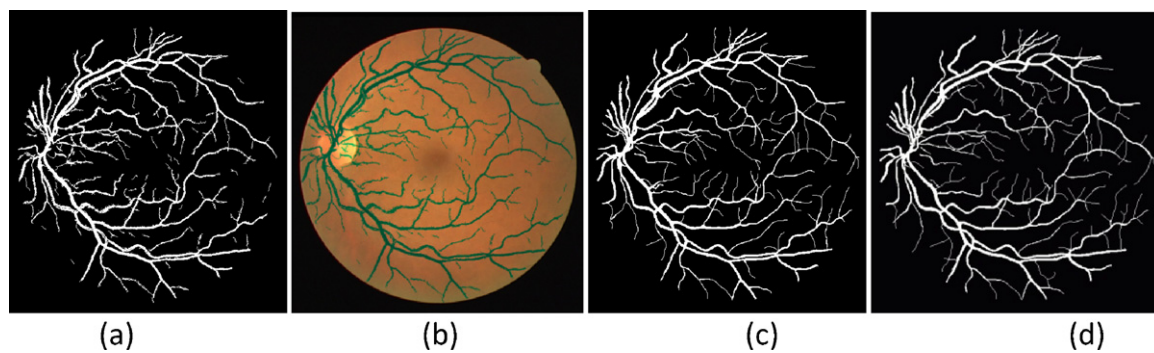


Fig. 5 – (a) Extracted vessel tree, (b) segmented vessels superimposed on colored image, (c) 1st human observer and (d) 2nd human observer.

per color plane at  $1440 \times 960$ ,  $2240 \times 1488$  or  $2304 \times 1536$  pixels. Out of these, 800 images are acquired with pupil dilation (one drop of Tropicamide at 0.5%) and 400 without dilation. The 20 randomly selected images in the 400 non-dilated image set are manually segmented twice by the two authors, resulting in a set A and a set B. The performance is computed with the segmentations of the set A as a ground truth. The comparison of set B with the ground truth image gives a detection

performance measure which is regarded as a target performance level.

#### 4.2. Performance measures

In the retinal vessel segmentation process, the outcome is a pixel-based classification result. Any pixel is classified either as vessel or surrounding tissue. Consequently, there are four



**Table 1 – Performance metrics for retinal vessel segmentation.**

Measure	Description
TRP	TP/vessel pixel count
FPR	FP/non-vessel pixel count
Specificity	TN/(TN + FP)
Sensitivity	TP/(TP + FN)
Accuracy	(TP + TN)/FOV pixel count
PPV	TP/(TP + FP)

events; two classifications and two misclassifications. The classifications are the True Positive (TP) where a pixel is identified as vessel in both the ground truth and segmented image, and the True Negative (TN) where a pixel is classified as a non-vessel in ground truth and segmented image. The two misclassifications are the False Negative (FN) where a pixel is classified as non-vessel in segmented image but as a vessel pixel in the ground truth image, and the False Positive (FP) where a pixel is marked as vessel in the segmented image but non-vessel in the ground truth image.

The performance metrics for retinal vessel segmentation are illustrated in Table 1. True Positive Rate (TPR) represents the fraction of pixels correctly detected as vessel pixels. False Positive Rate False Positive Rate (FPR) is the fraction of pixels erroneously detected as vessel pixels. The accuracy (Acc) is measured by the ratio of the total number of correctly classified pixels (sum of true positives and true negatives) by the number of pixels in the image FOV. Sensitivity (SN) reflects the ability of an algorithm to detect the vessel pixels. Specificity (SP) is the ability to detect non-vessel pixels. It can be expressed as  $1 - \text{FPR}$ . The Positive Predictive Value (PPV) or precession rate gives the proportion of identified vessel pixels which are true vessel pixels. It is the probability that an identified vessel pixel is a true positive.

### 4.3. Vessel segmentation results

The performance measures on the DRIVE, STRARE and MESSIDOR databases along with segmented vessel images are illustrated in this section. The performance of various monochromatic representations of different color spaces is also analyzed. Moreover, the methodology is also evaluated on noisy and pathological images. Finally, a comparison with other published methodologies is presented (Tables 7 and 8).

#### 4.3.1. Segmentation results

The average of the selected measures of performance which includes, the accuracy, true positive rate, false positive rate,

specificity and the precession rate for the DRIVE STARE and MESSIDOR databases is tabulated in Table 2.

The plot of selected performance measures for every image in the DRIVE, STARE and MESSIDOR databases is illustrated in Fig. 6.

The segmented retinal images from the DRIVE, STARE and MESSIDORE databases are illustrated in Table 3, where the original retinal image, the resulting vessel segmented image, the manually segmented images from the 1st human observer which is considered as the ground truth and the manual segmentation from the 2nd human observer are shown. The best case accuracy, TPR, FPR and PPV for the DRIVE database are 0.961942, 0.839999, 0.021225 and 0.845282, respectively and the worst case measures are 0.937794, 0.671040, 0.021144 and 0.830087, respectively. For the STARE database, the best case of vessel segmentation results is presented in the third row of Table 3, with the accuracy of 0.955241, TPR and FRP are 0.932185 and 0.042033, respectively, Specificity is 0.957967 and PPV is 0.723854. The image with the worst case of segmentation results is shown in the fourth row where the accuracy is 0.924064, TPR and FPR are 0.310690 and 0.006072, respectively. The best case of vessel segmentation results for the MESSIDOR database has an accuracy of 0.962618, TPR and FRP are 0.800087 and 0.023517, respectively, Specificity is 0.976483 and PPV is 0.743725. The worst case accuracy is 0.956755, TPR and FPR are 0.665296 and 0.015985, respectively. The complete set of segmented images is available at <http://studentnet.kingston.ac.uk/~k0961040/fodogj.html>.

#### 4.3.2. Evaluation with color channels

In this paper, several monochromatic representations of the original color images are investigated in order to evaluate their capability for the segmentation of the retinal vessels. The high contrast between vessels and their background has made the green channel of RGB a natural choice for this kind of application, but other alternatives are also possible depending upon the characteristics of the original color images. In this work, the representations we have analyzed are the green component of the original RGB image, the Intensity channel of the HSI color space, The luminosity channel of NTSC (YIQ) color space and the  $L^*$  component of the  $L^*A^*B^*$  representation; examples of these four representations are presented in Fig. 7. The one shown in top row is taken from the DRIVE database and the other in the bottom row is from the STARE database.

Table 4 shows the average accuracy, true positive rate, false positive rate, specificity and precision rate of the above mentioned color channels for vessel segmentation on the DRIVE, STARE and MESSIDOR database.

**Table 2 – Average performance measures on DRIVE, STARE and MESSIDOR.**

Database	Segmentation	Average accuracy	True positive rate	False positive rate	Specificity	PPV
DRIVE	2nd human observer	0.9470	0.7763	0.0276	0.9723	0.8066
	Proposed methodology	0.9430	0.7152	0.0231	0.9759	0.8150
STARE	2nd human observer	0.9348	0.8951	0.0615	0.9384	0.6425
	Proposed methodology	0.9442	0.7311	0.0319	0.9680	0.7413
MESSIDOR	2nd human observer	0.9693	0.8172	0.0150	0.9849	0.8419
	Proposed methodology	0.9579	0.7502	0.0214	0.9785	0.7770



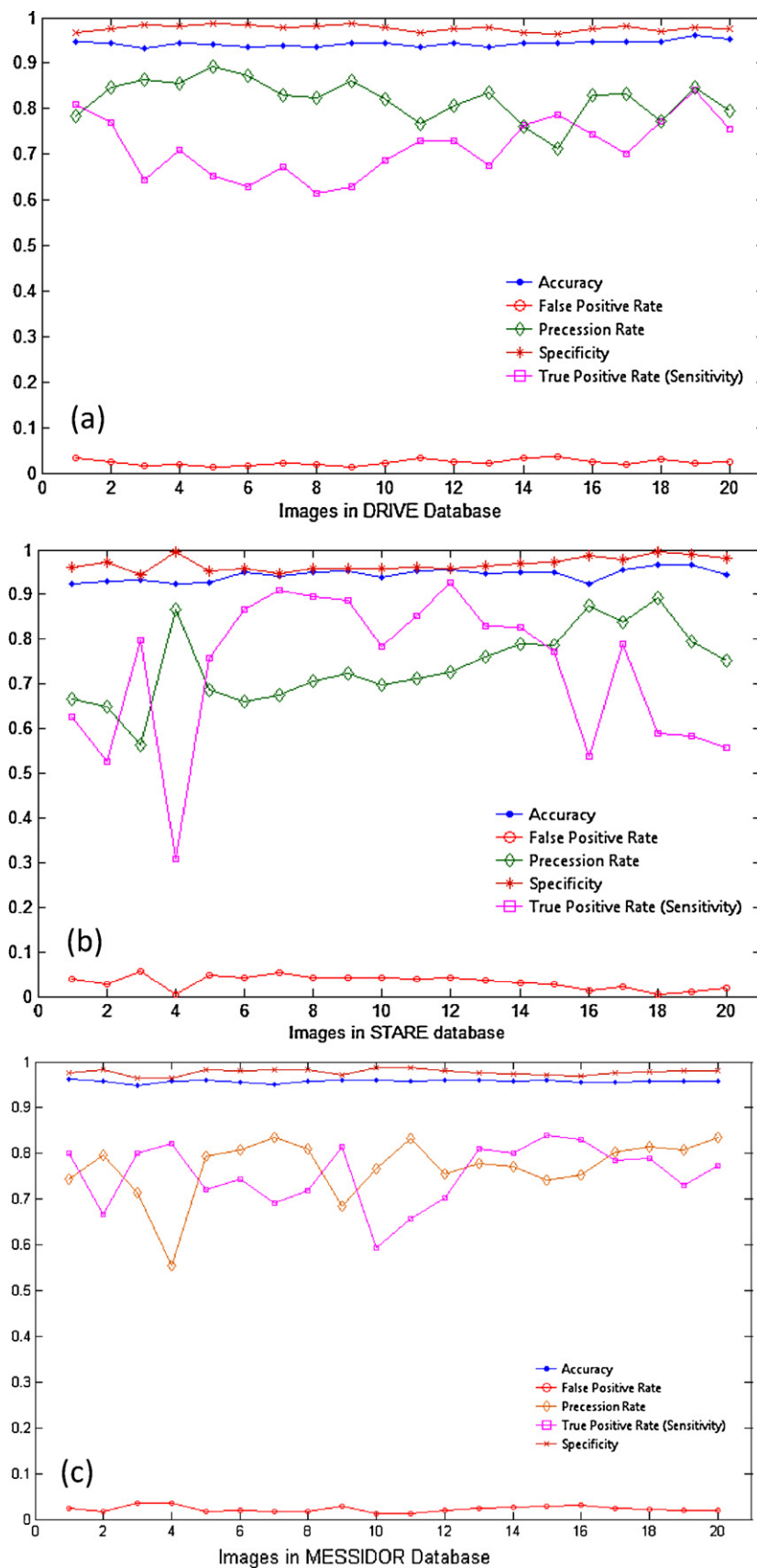

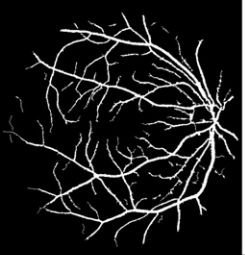
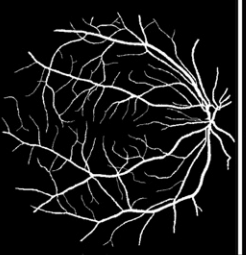


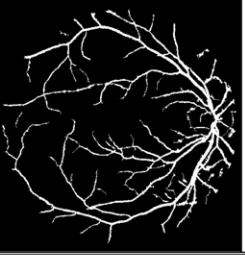
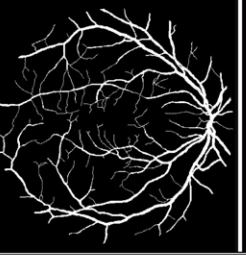
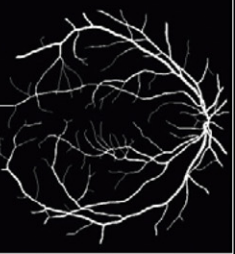
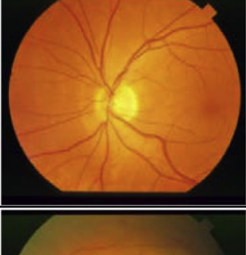
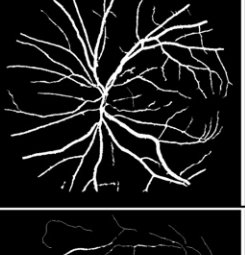
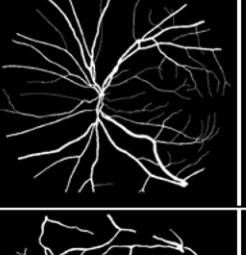
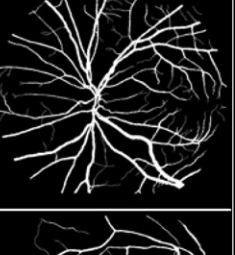
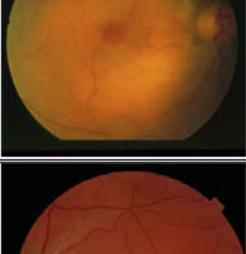
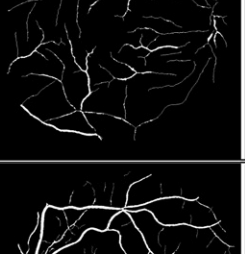
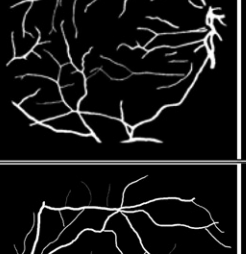
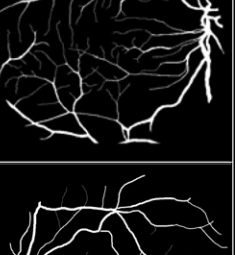
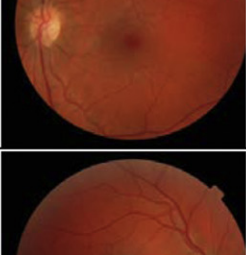

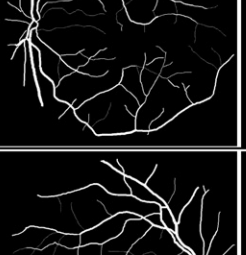
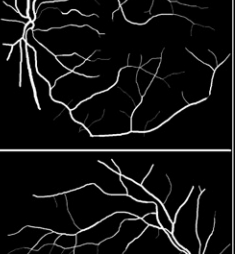
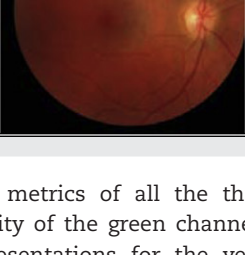
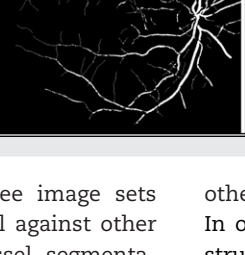
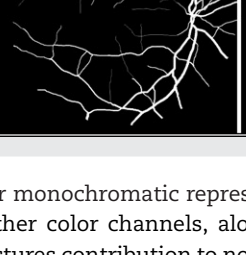
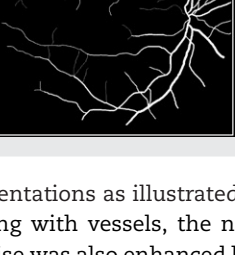


Fig. 6 – Performance measures on images from (a) DRIVE database, (b) STARE database and (c) MESSIDOR database.

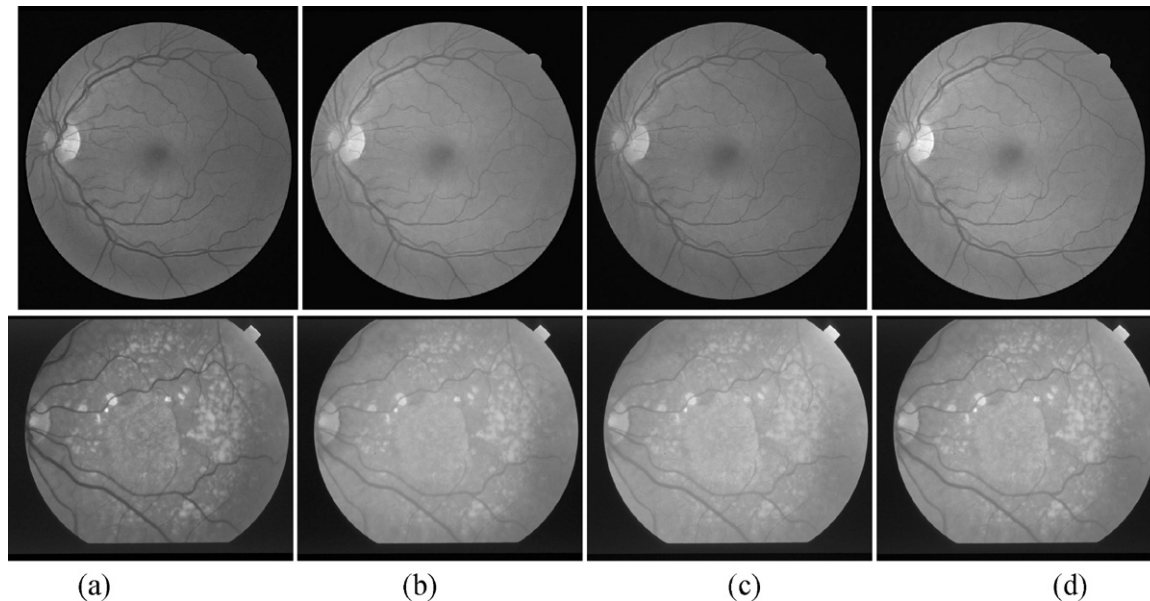
Table 3 – Segmentation results for DRIVE, STARE and MESSIDOR databases.

		Input image	Segmentation result	1 <sup>st</sup> human observer	2 <sup>nd</sup> human observer
DRIVE	Best case				
	Worst case				
STARE	Best case				
	Worst case				
MESSIDORE	Best case				
	Worst case				

The performance metrics of all the three image sets indicate the superiority of the green channel against other monochromatic representations for the vessel segmentation task. The reason is that the enhancement of vessel structures with suppression of non vessel objects including background with the morphological top-hat transformation is more noticeable with the green channel as compared to the

other monochromatic representations as illustrated in Fig. 8. In other color channels, along with vessels, the non-vessel structures contribution to noise was also enhanced leading to an increase in the number of false positives, thus decreasing the accuracy.

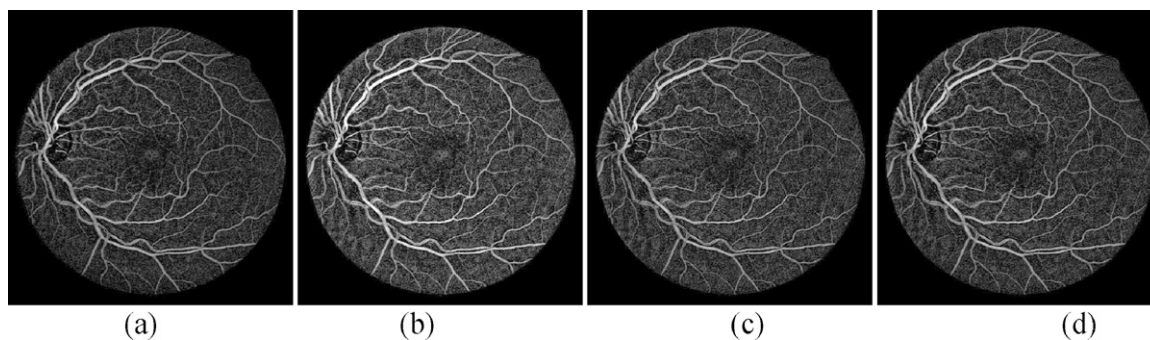
We have also evaluated the selected monochromatic representations for vessel segmentation in such a way that the



**Fig. 7 – Monochromatic representations (a) Green channel of RGB, (b)  $L^*$  of  $L^*A^*B^*$ , (c) I component of HSI and (d) luminance channel of NTSC.**

**Table 4 – Performance measures for color channels in vessel segmentation.**

Database	Color channel	Average accuracy	True positive rate	False positive rate	Specificity	PPV
DRIVE	Green channel of RGB	0.942366	0.716161	0.024100	0.975900	0.815018
	I component of HIS	0.939063	0.691526	0.024444	0.975556	0.809716
	$L^*$ component of $L^*A^*B^*$	0.940007	0.631292	0.014392	0.985608	0.866060
	Luminosity channel of NTSC (YIQ)	0.941797	0.703580	0.023068	0.976932	0.820551
STARE	Green Channel of RGB	0.944184	0.731088	0.031946	0.968054	0.741356
	I component of HIS	0.943335	0.700794	0.029610	0.970390	0.749728
	$L^*$ Component of $L^*A^*B^*$	0.933020	0.611872	0.030972	0.969028	0.715733
	Luminosity Channel of NTSC (YIQ)	0.943897	0.721217	0.031147	0.968853	0.744607
MESSIDOR	Green Channel of RGB	0.957883	0.75025	0.021470	0.978530	0.777035
	I component of HIS	0.952546	0.650395	0.017894	0.982106	0.787050
	$L^*$ Component of $L^*A^*B^*$	0.944667	0.465417	0.007839	0.992161	0.868624
	Luminosity Channel of NTSC (YIQ)	0.956614	0.743722	0.022533	0.977467	0.769790



**Fig. 8 – Sum of top-hat transformation for (a) Green channel of RGB, (b)  $L^*$  of  $L^*A^*B^*$ , (c) I component of HSI and (d) luminance channel of NTSC.**

vessel centerlines are extracted using the respective color channel whereas the vessel shape and orientation maps are generated from the green channel of RGB and the final segmented image is obtained by the reconstruction of these two images. That means the differential filtering for vessel

skeleton detection is performed on the respective color channel and the morphological bit plane slicing is applied on the green channel of RGB, and the segmented vessel tree is obtained by using these two images. The performance measures of the segmentation results with the use of different

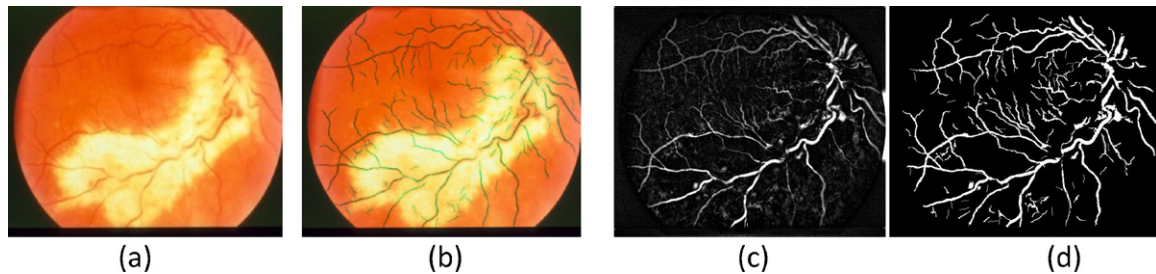
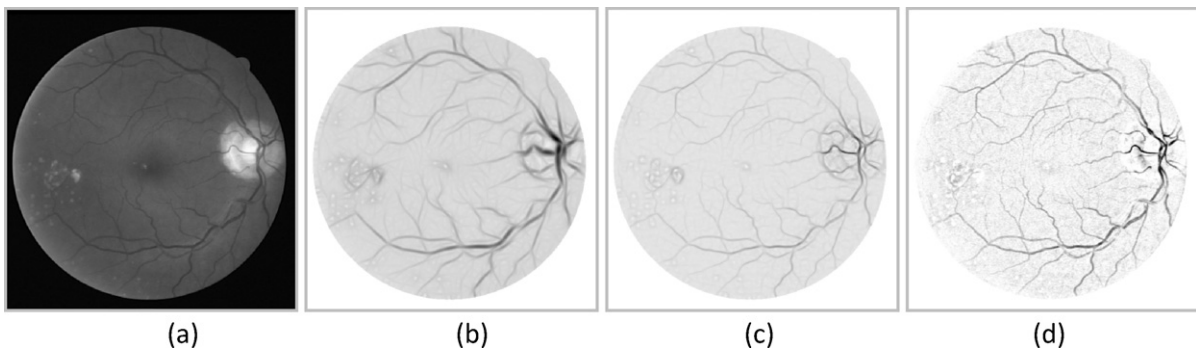


**Table 5 – Vessel segmentation performance metrics; color channels used for skeleton detection and green channel is used for vessel map generation.**

Database	Color channel for vessel skelton detection	Average accuracy	True positive rate	False positive rate	Specificity	PPV
DRIVE	L* component of L*A*B*	0.943098	0.715235	0.023117	0.976883	0.820585
	I component of HSI	0.942814	0.715577	0.023535	0.976465	0.818297
	Luminosity channel of NTSC (YIQ)	0.942735	0.717110	0.023829	0.976171	0.816497
STARE	L* component of L*A*B*	0.943731	0.718267	0.030994	0.969006	0.744296
	I component of HSI	0.943335	0.700794	0.029610	0.970390	0.749728
	Luminosity channel of NTSC (YIQ)	0.943897	0.721217	0.031147	0.968853	0.744607
MESSIDOR	L* component of L*A*B*	0.958650	0.736619	0.019386	0.980614	0.792045
	I component of HSI	0.958433	0.737076	0.019642	0.980358	0.789925
	Luminosity channel of NTSC (YIQ)	0.958447	0.746749	0.020508	0.979492	0.784500

**Table 6 – Performance measures with noise models (DRIVE database).**

Noise model	Average accuracy	True positive rate	False positive rate	Specificity	PPV
Gaussian noise with 0.5 mean and 0.0001 variance	0.9301	0.7741	0.04629	0.9537	0.7155
Salt and pepper noise with density 0.002	0.9427	0.7184	0.02345	0.9765	0.8218
Speckle multiplicative noise with 0.0005 variance	0.9322	0.7628	0.04218	0.9641	0.7337

**Fig. 9 – Pathological Image from STARE database (a) colored image, (b) centerlines superimposed on colored image, (c) sum of top-hat and (d) final segmented image.****Fig. 10 – (a) The green channel of retinal image with pathologies, (b)–(d) vessel features computed from gabor filter, line strength and morphological operator, respectively.**

color channels for centerlines detection and the green channel for vessel map generation are illustrated in Table 5 for the DRIVE, STARE and MESSIDOR databases.

It has been observed that the green channel of RGB is more suitable for morphological operations than the other monochromatic representations whereas, for differential filtering, the performance of other color channels is comparable. This is deduced from the increase in average accuracy, TPR, FPR and precision rates for HIS and L\*A\*B when the green

channel generated vessel shape and orientation map is used with the centerlines extracted from HIS and L\*A\*B\* for reconstruction of the final segmentation of the vessel tree. For the STARE database, an interesting observation is that the centerlines detected using the green channel of RGB is almost identical with the centerlines detected using the “I” component of HIS and the luminosity channel of NTSC, therefore the performance measures shown for these color channels in Table 5 are similar to those illustrated in Table 4.



**Table 7 – Performance comparison of vessel segmentation methods (DRIVE images).**

Sr. No.	Methods	Average accuracy (standard deviation)	True positive rate (Kappa)	False positive rate	Specificity
1	2nd human observer	0.9470 (0.0048)	0.7763	0.0276	0.9725
2	Zana and Klein [47]	0.9377 (0.0077)	0.6971	N.A	N.A
3	Abramoff et al. [27]	0.9416 (0.0065)	0.7145	0.0304	0.9696
4	Xiaoyi and Mojon [38]	0.9212 (0.0076)	0.6399	N.A	N.A
5	Al-Diri et al. [75]	0.9258 (0.0126)	0.6716	N.A	N.A
6	Martinez-Perez et al. [58]	0.9181 (0.0240)	0.6389	N.A	N.A
7	Chaudhuri et al. [20]	0.8773 (0.0232)	0.3357	N.A	N.A
8	Mendonca and Campilho [15]	0.9452 (0.0062)	0.7344	0.0236	0.9764
9	Soares et al. [28]	0.9466 (0.0058)	0.7285	0.0213	0.9786
10	Staal et al. [14]	0.9441 (0.0065)	0.7345	N.A	N.A
11	Ricci and Perfetti [29]	0.9595	N.A	N.A	N.A
12	Lam et al. [70]	0.9472	N.A	N.A	N.A
13	Fraz et al. [83]	0.9303 (0.0079)	0.7114	0.0320	0.9680
14	Proposed method	0.9430 (0.0072)	0.7152	0.0231	0.9768

N.A., not available.

**Table 8 – Performance comparison of vessel segmentation methods (STARE images).**

Sr. No.	Methods	Average accuracy	True positive rate	False positive rate	Specificity
1	2nd human observer	0.9348	0.8951	0.06157	0.9384
2	Hoover et al. [37]	0.9267	0.6751	0.0433	0.9567
3	Xiaoyi and Mojon [38]	0.9009	N.A	N.A	N.A
4	Staal et al. [14]	0.9516	0.6970	0.0190	0.9810
5	Soares et al. [28]	0.9478	0.7197	0.02529	0.9747
6	Mendonca and Campilho [15]	0.9440	0.6996	0.0270	0.9730
7	Fraz et al. [83]	0.9367	0.6849	0.0290	0.9710
8	Lam and Hong [18]	0.9474	N.A	N.A	N.A
9	Lam et al. [70]	0.9567	N.A	N.A	N.A
10	Ricci and Perfetti [29]	0.9646	N.A	N.A	N.A
11	Proposed Method	0.9442	0.7311	0.03194	0.968054

N.A., not available.

#### 4.3.3. Evaluation with noisy/pathological images

The methodology is tested for robustness in the presence of noise as well as on pathological images. The noise models typically found in biomedical images are Gaussian, salt and Pepper and speckle multiplicative noise [82]. All of the twenty test images of the DRIVE database are corrupted with these models before segmentation. The performance measures shown in Table 6 indicate a slight decrease in accuracy for Gaussian and speckle noise due to increased false positive rate. The methodology is shown to be insensitive to the salt and pepper noise.

Retinal image pathologies are successfully taken care of by the morphological top-hat transformation. The morphological top-hat transformation uses an oriented line shape structuring element, therefore every isolated round shaped and bright pathological regions whose diameter is less than the length of linear structuring element are not enhanced and thus removed from the retinal image. The sum of top-hat on the filtered image will enhance all vessels whatever their direction, including small or tortuous vessels. The large homogeneous pathological areas will not be enhanced since they are unchanged by the transformation as revealed in Fig. 9.

A retinal image containing pathologies is illustrated from the DRIVE database in Fig. 10. The green channel is shown in Fig. 10(a). There is a ringing effect visible around the

boundary of pathologies in the images obtained by Soares' Gabor filter [28] and the Ricci's line strength measure [29], which contributes towards false positives. The output of the sum of top hat transformation is shown in Fig. 10(d) where the ringing effect across the pathological boundary is not present.

#### 4.3.4. Comparison with published methods

The performance of the proposed methodology is compared with 13 published algorithms for DRIVE and ten methods for STARE in Tables 7 and 8, respectively. The maximum average accuracy, true positive rate, false positive rate and specificity are calculated for the test set of each of the databases, using the green channel of the RGB images. The same performance measures for other vessel segmentation methods are obtained from the respective publications.

## 5. Discussions and conclusions

An automated segmentation method of identifying blood vessels in retinal images has been proposed in this paper. This methodology employs a novel combination of different image processing techniques which encompasses the use of the FoDoG filter for detection of vessel centerlines aggregated with the application of multidirectional morphological bit plane

slicing. The skeleton of the blood vessels is acquired by detecting vessel centerlines. The shape and orientation maps are generated by the application of a multidirectional top-hat operator with a linear oriented structuring element which emphasizes the vessels in a particular direction and later significant information is extracted from the grayscale image using bit plane slicing. The final vessel tree is obtained by reconstruction of the vessel centerlines and the shape and orientation maps.

The methodology has been tested on two established publicly available databases (DRIVE and STARE) and a new public database (MESSIDOR). Different monochromatic representations of retinal images have also been tested and evaluated for their suitability for vessel segmentation. Experimental results show that the values of performance measures achieved with the proposed methodology are comparable, and in some cases, even exceed recently published results, and approximate to the performance of human observers. It is noteworthy that the average values for true positives (sensitivity) and specificity, which assess the agreement of the individual pixel classification with the ground truth vessel and non vessel classes, respectively, are, in most cases, higher than those reported by other authors.

The adequacy of other monochromatic representations for vessel segmentation is also evaluated and it is evident that the Luminance Channel of NTSC (YIQ) color space is a good alternative for the green channel of RGB. The average accuracy, the true positive rate and false positive rate achieved with the luminosity image is comparable with the green channel for both DRIVE and STARE databases. The FoDoG filter which is used for centerline detection is less sensitive to the background noise which is more intense in the green channel image as compared to the luminance image as shown in Fig. 7. Therefore, when other monochromatic representations are used for the application of the centerline detection algorithm and the green channel is used for vessel map generation, then the performance measures of vessel segmentation are increased as compared to the case when the complete methodology is applied only to the green channel or only to the respective monochromatic representation. This conclusion is illustrated in Table 5, where an increase in the accuracy, true positive, false positive and precision rates for the “I” component of HIS, the luminosity channel of NTSC and  $L^*$  of  $L^*A^*B^*$  is observed as compared to the results shown in Table 4.

There is significant disagreement in the identification of vessels even amongst expert observers as reflected in the accuracy and sensitivity of the 2nd human observer. As, illustrated in Table 7, the average accuracy of the proposed algorithm is 0.9430 with a true positive rate and false positive rate of 0.7152 and 0.0231, respectively. The proposed approach surpasses the previous work [83] in terms of accuracy by 1.36%, true positive rate i.e. the sensitivity by 0.53% and the false positive rate is decreased by 38.52%. In terms of average accuracy, the proposed method is better than Xiaoyi and Mojon [38], Martinez-Perez et al. [58], Al-Diri et al. [75] and Chaudhuri et al. [20], Abramoff et al. [27] and Zana and Klein [47] (2.36%, 2.71%, 1.8%, 7.48%, 0.14%, 0.565%, respectively). This algorithm has achieved higher true positive rate than Xiaoyi and Mojon [38], Martinez-Perez et al. [58], Al-Diri et al. [75], Abramoff et al. [27], Zana and Klein [47] and Fraz et al. [83] (11.76%, 11.94%, 6.49%,

0.01%, 2.59%, 0.53%, respectively). For the STARE dataset, the average accuracy produced by this algorithm is 0.9441 with a true positive rate and false positive rate of 0.7310 and 0.0319, respectively. There is an improvement in the results of this algorithm as compared to previous work [83] in accuracy and true positive rate by 0.8% and 6.74%, respectively. The average accuracy achieved by this algorithm exceeds the accuracy of the 2nd human observer by 0.94%, Hoover by 1.88%, Xiaoyi and Mojon [38] by 4.80%, Mendonca and Campilho [15] by 0.02%. As expected, the average segmentation accuracy of two supervised methods Staal et al. [14] and Soares et al. [28] is higher than this algorithm, but as mentioned by Staal et al. [14], they used only 19 (ten normal and nine with pathology) of the 20 images in the STARE database. The algorithms presented by Ricci and Perfetti [29] and Lam et al. [18,70] are state of the art methodologies of vessel segmentation from pathological retinal images and their reported accuracy is higher than this algorithm. The methodology presented by Lam incorporated the multi-concavity models for different types of retinal pathologies including bright and dark lesions simultaneously. The concavity measures are combined according to their statistical and geometrical properties and later a lifting technique is used for optimizing the regularized solution towards the ideal vessel shape. This approach greatly reduces the detection of false positives hence increase in accuracy. Ricci and Perfetti [29] employed two orthogonal line detectors in twelve orientations to construct a three dimensional feature vector for supervised classification using a support vector machine. With respect to other supervised techniques, the algorithm (1) requires fewer features, (2) feature extraction is computationally simpler, and (3) fewer examples are needed for training. The algorithm makes use of local differential computation of the line strength which makes the line detector robust with respect to non-uniform illumination and contrast. Also the line detector behavior in the presence of a central reflex is satisfactory. These attributes combined with supervised classification using SVM resulted in significant reduction of the false positive detection hence an increase in accuracy of the algorithm. Enhancements to the proposed methodology with respect to its performance on images that contain pathology are planned for future work. It is expected, that as with the Ricci and Perfetti [29] and Lam et al. [18,70] methodologies, the models for retinal pathologies and central vessel reflex will need to be incorporated into the algorithm in relation to this application.

The first twenty images from the MESSIDOR dataset (Base31) are analyzed using the proposed method. MESSIDOR is relatively new database and ground truths are not available with respect to blood vessels. Ground truths of these images have been created by two authors using Live-vessel software [54]. The proposed algorithm produced promising results on this database as shown in Tables 2 and 3. The average accuracy achieved by the proposed method for MESSIDOR images is 0.9573 with TPR, FPR, specificity and PPV of 0.7540, 0.0224, 0.9775, and 0.7698, respectively.

In Fig. 6(a), the selected performance measures of all the images of the DRIVE database is plotted, with the range shown from 0.932 to 0.965 for accuracy, 0.66 to 0.83 for TPR, 0.01 to 0.06 for FPR and 0.73 to 0.89 for precision rate. These performance measures are also plotted for the STARE database in

Fig. 6(b), where the range of accuracy is 0.923–0.968, the TPR are between 0.313 and 0.917, the FPR ranges between 0.005 and 0.0612 and precession rate is from 0.57 to 0.87. It is observed that the true positives and false positives of “Im004.tif” in the STARE database are very small, indicating the low vessel detection rate which is illustrated in the fourth row of Table 3. These performance measures are also plotted for images of the MESSIDOR database in Fig. 6(c), where it can be observed that the accuracy ranges between 0.9610 and 0.9756, which is the best amongst the results.

The segmented vascular tree depends upon the detection of vessel centerlines and the vessel shape and orientation maps. The centerline detection algorithm is based on the fact that the maximum local intensity across a blood vessel cross-section profile in the retina generally occurs at the vessel center pixels and the vessel centerlines are measured as the connected sets of pixels which correspond to intensity maxima computed from the intensity profiles of the vessel cross sections. This assumption works perfectly with the vessels featuring the Gaussian shaped profile. However, these methods appear less suited to retinal images where arterioles show prominent light reflexes (e.g. in images of younger participants). The application of first order derivative of Gaussian for centerlines detection on such images results in the detection of two lines running parallel to each other located just inside the edges of the blood vessel. The application of a dual Gaussian profile or hermite polynomial shaped model to images in children with prominent vessel reflexes is the topic of future work.

## REFERENCES

- [1] H. Leung, J.J. Wang, E. Rochtchina, A.G. Tan, T.Y. Wong, R. Klein, L.D. Hubbard, P. Mitchell, Relationships between age, blood pressure, and retinal vessel diameters in an older population, *Investigative Ophthalmology and Visual Science* 44 (2003) 2900–2904.
- [2] T.Y. Wong, R. Klein, A.R. Sharrett, B.B. Duncan, D.J. Couper, J.M. Tielsch, B.E.K. Klein, L.D. Hubbard, Retinal arteriolar narrowing and risk of coronary heart disease in men and women, *JAMA: The Journal of the American Medical Association* 287 (2002) 1153–1159.  
<http://jama.ama-assn.org/content/287/9/1153.abstract>.
- [3] T. Teng, M. Lefley, D. Claremont, Progress towards automated diabetic ocular screening: A review of image analysis and intelligent systems for diabetic retinopathy, *Medical and Biological Engineering and Computing* 40 (2002) 2–13.
- [4] C. Heneghan, J. Flynn, M. O’Keefe, M. Cahill, Characterization of changes in blood vessel width and tortuosity in retinopathy of prematurity using image analysis, *Medical Image Analysis* 6 (2002) 407–429.
- [5] A. Haddouche, M. Adel, M. Rasigni, J. Conrath, S. Bourennane, Detection of the foveal avascular zone on retinal angiograms using Markov random fields, *Digital Signal Processing* 20 (2010) 149–154.
- [6] E. Grisan, A. Ruggeri, A divide et impera strategy for automatic classification of retinal vessels into arteries and veins. *Engineering in Medicine and Biology Society*, 2003. Proceedings of the 25th Annual International Conference of the IEEE, 2003.
- [7] M. Foracchia, Extraction and quantitative description of vessel features in hypertensive retinopathy fundus images, in: E. Grisan (Ed.), *Book Abstracts 2nd International Workshop on Computer Assisted Fundus Image Analysis*, 2001, p. 6.
- [8] J. Lowell, A. Hunter, D. Steel, A. Basu, R. Ryder, R.L. Kennedy, Measurement of retinal vessel widths from fundus images based on 2-D modeling, *IEEE Transactions on Medical Imaging* 23 (2004) 1196–1204.
- [9] J.J. Kanski, *Clinical Ophthalmology*, 6th ed., Elsevier Health Sciences, London, UK, 2007.
- [10] F. Zana, J.C. Klein, A multimodal registration algorithm of eye fundus images using vessels detection and Hough transform, *IEEE Transactions on Medical Imaging* 18 (1999) 419–428.
- [11] K. Fritzsche, A. Can, H. Shen, C. Tsai, J. Turner, H.L. Tanenbaum, C.V. Stewart, B. Roysam, J.S. Suri, S. Laxminarayan, Automated model based segmentation, tracing and analysis of retinal vasculature from digital fundus images, in: J.S. Suri, S. Laxminarayan (Eds.), *State-of-The-Art Angiography, Applications and Plaque Imaging Using MR, CT, Ultrasound and X-rays*, Academic Press, 2003, pp. 225–298.
- [12] L. Huiqi, O. Chutatape, Automated feature extraction in color retinal images by a model based approach, *IEEE Transactions on Biomedical Engineering* 51 (2004) 246–254.
- [13] C. Mariño, G. Penedo, M. Penas, J. Carreira, F. Gonzalez, Personal authentication using digital retinal images, *Pattern Analysis and Application* 9 (2006) 21–33.
- [14] J. Staal, M.D. Abramoff, M. Niemeijer, M.A. Viergever, B. van Ginneken, Ridge-based vessel segmentation in color images of the retina, *IEEE Transactions on Medical Imaging* 23 (2004) 501–509.
- [15] A.M. Mendonca, A. Campilho, Segmentation of retinal blood vessels by combining the detection of centerlines and morphological reconstruction, *IEEE Transactions on Medical Imaging* 25 (2006) 1200–1213.
- [16] K. Sun, Z. Chen, S. Jiang, Y. Wang, Morphological multiscale enhancement, fuzzy filter and watershed for vascular tree extraction in angiogram, *Journal of Medical Systems* (2010), doi:10.1007/s10916-010-9466-3,  
<http://www.springerlink.com/content/e82n0944n6223004/>.
- [17] M. Sofka, C.V. Stewart, Retinal vessel centerline extraction using multiscale matched filters, confidence and edge measures, *IEEE Transactions on Medical Imaging* 25 (2006) 1531–1546.
- [18] B.S.Y. Lam, Y. Hong, A novel vessel segmentation algorithm for pathological retina images based on the divergence of vector fields, *IEEE Transactions on Medical Imaging* 27 (2008) 237–246.
- [19] L. Espona, M.J. Carreira, M. Ortega, M.G. Penedo, A Snake for Retinal Vessel Segmentation. *Proceedings of the 3rd Iberian conference on Pattern Recognition and Image Analysis, Part II*, Springer-Verlag, Girona, Spain, 2007.
- [20] S. Chaudhuri, S. Chatterjee, N. Katz, M. Nelson, M. Goldbaum, Detection of blood vessels in retinal images using two-dimensional matched filters, *IEEE Transactions on Medical Imaging* 8 (1989) 263–269.
- [21] DRIVE, Digital Retinal Images for Vessel Extraction.  
<http://www.isi.uu.nl/Research/Databases/DRIVE/>, 2004.
- [22] STARE, Structured Analysis of the Retina.  
<http://www.ces.clemson.edu/~ahoover/stare/>, 2000.
- [23] MESSIDOR, Methods for Evaluating Segmentation and Indexing techniques Dedicated to Retinal Ophthalmology.  
<http://messidor.crihan.fr/index-en.php>, 2004.
- [24] K. Akita, H. Kuga, A computer method of understanding ocular fundus images, *Pattern Recognition* 15 (1982) 431–443.
- [25] R. Nekovei, S. Ying, Back-propagation network and its configuration for blood vessel detection in angiograms, *IEEE Transactions on Neural Networks* 6 (1995) 64–72.

- [26] C. Sinthanayothin, J.F. Boyce, H.L. Cook, T.H. Williamson, Automated localisation of the optic disc, fovea, and retinal blood vessels from digital colour fundus images, *British Journal of Ophthalmology* 83 (1999) 902–910.
- [27] M. Niemeijer, J.J. Staal, B. van Ginneken, M. Loog, M.D. Abramoff, Comparative study of retinal vessel segmentation methods on a new publicly available database. *SPIE Medical Imaging* 5374 (2004) 648–656.
- [28] J.V.B. Soares, J.J.G. Leandro, R.M. Cesar, H.F. Jelinek, M.J. Cree, Retinal vessel segmentation using the 2-D Gabor wavelet and supervised classification, *IEEE Transactions on Medical Imaging* 25 (2006) 1214–1222.
- [29] E. Ricci, R. Perfetti, Retinal blood vessel segmentation using line operators and support vector classification, *IEEE Transactions on Medical Imaging* 26 (2007) 1357–1365.
- [30] A. Osareh, B. Shadgar, Automatic blood vessel segmentation in color images of retina, *Iranian Journal of Science and Technology Transaction B-Engineering* 33 (2009) 191–206.
- [31] C.A. Lupascu, D. Tegolo, E. Trucco, FABC: Retinal vessel segmentation using AdaBoost, *IEEE Transactions on Information Technology in Biomedicine* 14 (2010) 1267–1274.
- [32] Y.A. Tolias, S.M. Panas, A fuzzy vessel tracking algorithm for retinal images based on fuzzy clustering, *IEEE Transactions on Medical Imaging* 17 (1998) 263–273.
- [33] S. Salem, N. Salem, A. Nandi, Segmentation of retinal blood vessels using a novel clustering algorithm (RACAL) with a partial supervision strategy, *Medical and Biological Engineering and Computing* 45 (2007) 261–273.
- [34] J. Ng, S.T. Clay, S.A. Barman, A.R. Fielder, M.J. Moseley, K.H. Parker, C. Paterson, Maximum likelihood estimation of vessel parameters from scale space analysis, *Image and Vision Computing* 28 (2010) 55–63.
- [35] G.B. Kande, P.V. Subbaiah, T.S. Savithri, Unsupervised fuzzy based vessel segmentation in pathological digital fundus images, *Journal of Medical Systems* 34 (2009) 849–858.
- [36] F. Villalobos-Castaldi, E. Felipe-Riverón, L. Sánchez-Fernández, A fast, efficient and automated method to extract vessels from fundus images, *Journal of Visualization* 13 (2010) 263–270.
- [37] A.D. Hoover, V. Kouznetsova, M. Goldbaum, Locating blood vessels in retinal images by piecewise threshold probing of a matched filter response, *IEEE Transactions on Medical Imaging* 19 (2000) 203–210.
- [38] J. Xiaoyi, D. Mojon, Adaptive local thresholding by verification-based multithreshold probing with application to vessel detection in retinal images, *IEEE Transactions on Pattern Analysis and Machine Intelligence* 25 (2003) 131–137.
- [39] C. Yao, H.-j. Chen, Automated retinal blood vessels segmentation based on simplified PCNN and fast 2D-Otsu algorithm, *Journal of Central South University of Technology* 16 (2009) 640–646.
- [40] W.T. Freeman, E.H. Adelson, The Design and Use of Steerable Filters, *IEEE Transactions on Pattern Analysis and Machine Intelligence* 13 (1991) 891–906.
- [41] B. Kochner, D. Schuhmann, M. Michaelis, G. Mann, K.-H. Englmeier, Course tracking and contour extraction of retinal vessels from color fundus photographs: Most efficient use of steerable filters for model-based image analysis, *Medical Imaging, Image Processing*, San Diego, CA, USA, 1998.
- [42] L. Gang, O. Chutatape, S.M. Krishnan, Detection and measurement of retinal vessels in fundus images using amplitude modified second-order Gaussian filter, *IEEE Transactions on Biomedical Engineering* 49 (2002) 168–172.
- [43] B. Zhang, L. Zhang, L. Zhang, F. Karay, Retinal vessel extraction by matched filter with first-order derivative of Gaussian, *Computers in Biology and Medicine* 40 (2010) 438–445.
- [44] M. Al-Rawi, M. Qutaishat, M. Arrar, An improved matched filter for blood vessel detection of digital retinal images, *Computers in Biology and Medicine* 37 (2007) 262–267.
- [45] M.G. Cinsdikici, D. Aydin, Detection of blood vessels in ophthalmoscope images using MF/ant (matched filter/ant colony) algorithm, *Computer Methods and Programs in Biomedicine* 96 (2009) 85–95.
- [46] M. Amin, H. Yan, High speed detection of retinal blood vessels in fundus image using phase congruency, *Soft Computing – A Fusion of Foundations, Methodologies and Applications* 15 (6) (2011) 1–14.
- [47] F. Zana, J.C. Klein, Segmentation of vessel-like patterns using mathematical morphology and curvature evaluation, *IEEE Transactions on Image Processing* 10 (2001) 1010–1019.
- [48] G. Ayala, T. Leon, V. Zapater, Different averages of a fuzzy set with an application to vessel segmentation, *IEEE Transactions on Fuzzy Systems* 13 (2005) 384–393.
- [49] I. Liu, Y. Sun, Recursive tracking of vascular networks in angiograms based on the detection-deletion scheme, *IEEE Transactions on Medical Imaging* 12 (1993) 334–341.
- [50] Z. Liang, M.S. Rzeszutarski, L.J. Singerman, J.M. Chokreff, The detection and quantification of retinopathy using digital angiograms, *IEEE Transactions on Medical Imaging* 13 (1994) 619–626.
- [51] O. Chutatape, Z. Liu, S.M. Krishnan, Retinal blood vessel detection and tracking by matched Gaussian and Kalman filters. *Engineering in Medicine and Biology Society, 1998. Proceedings of the 20th Annual International Conference of the IEEE, 1998.*
- [52] F.K.H. Quek, C. Kirbas, Vessel extraction in medical images by wave-propagation and traceback, *IEEE Transactions on Medical Imaging* 20 (2001) 117–131.
- [53] C. Ali, S. Hong, J.N. Turner, H.L. Tanenbaum, B. Roysam, Rapid automated tracing and feature extraction from retinal fundus images using direct exploratory algorithms, *IEEE Transactions on Information Technology in Biomedicine* 3 (1999) 125–138.
- [54] P. Kelvin, H. Ghassan, A. Rafeef, Live-vessel: extending livewire for simultaneous extraction of optimal medial and boundary paths in vascular images, in: *Proceedings of the 10th international conference on Medical image computing and computer-assisted intervention*, Springer-Verlag, Brisbane, Australia, 2007.
- [55] A.F. Frangi, W.J. Niessen, K.L. Vincken, M.A. Viergever, W. William, C. Alan, D. Scott, Live-vessel: extending livewire for simultaneous extraction of optimal medial and boundary paths in vascular images, in: *Lecture Notes in Computer Science. Proceedings of the 10th international conference on Medical image computing and computer-assisted intervention MICCAI™98*, vol. 1496, Springer, Berlin, Heidelberg, 1998, p. 130.
- [56] W.A. Barrett, E.N. Mortensen, Interactive live-wire boundary extraction, *Medical Image Analysis* 1 (1997) 331–341.
- [57] K.K. Delibasis, A.I. Kechriniotis, C. Tsonos, N. Assimakis, Automatic model-based tracing algorithm for vessel segmentation and diameter estimation, *Computer Methods and Programs in Biomedicine* 100 (2010) 108–122.
- [58] M.E. Martinez-Perez, A.D. Hughes, A.V. Stanton, S.A. Thom, A.A. Bharath, K.H. Parker, Retinal blood vessel segmentation by means of scale-space analysis and region growing. *Proceedings of the Second International Conference on Medical Image Computing and Computer-Assisted Intervention*, London, UK, 1999.
- [59] M.E. Martinez-Perez, A.D. Hughes, S.A. Thom, A.A. Bharath, K.H. Parker, Segmentation of blood vessels from red-free and fluorescein retinal images, *Medical Image Analysis* 11 (2007) 47–61.



- [60] L. Ibanez, W. Schroeder, L. Ng, J. Cates, The ITK Software Guide. <http://www.itk.org/ItkSoftwareGuide.pdf>: Kitware, Inc. ISBN 1-930934-10-6, 2003.
- [61] M.A. Palomera-Perez, M.E. Martinez-Perez, H. Benitez-Perez, J.L. Ortega-Arjona, Parallel multiscale feature extraction and region growing: Application in retinal blood vessel detection, *IEEE Transactions on Information Technology in Biomedicine* 14 (2010) 500–506.
- [62] O. Wink, W.J. Niessen, M.A. Viergever, Multiscale vessel tracking, *IEEE Transactions on Medical Imaging* 23 (2004) 130–133.
- [63] M. Vlachos, E. Dermatas, Multi-scale retinal vessel segmentation using line tracking, *Computerized Medical Imaging and Graphics* 34 (2009) 213–227.
- [64] K.A. Vermeer, F.M. Vos, H.G. Lemij, A.M. Vossepoel, A model based method for retinal blood vessel detection, *Computers in biology and medicine* 34 (2004) 209–219.
- [65] V. Mahadevan, H. Narasimha-Iyer, B. Roysam, H.L. Tanenbaum, Robust model-based vasculature detection in noisy biomedical images, *IEEE Transactions on Information Technology in Biomedicine* 8 (2004) 360–376.
- [66] P.J. Huber, A robust version of the probability ratio test, *The Annals of Mathematical Statistics* 36 (1965) 1753–1758.
- [67] C. Field, B. Smith, Robust estimation – A weighted maximum-likelihood approach, *International Statistical Review* 62 (1994) 405–424.
- [68] E. Ronchetti, Robust model selection in regression, *Statistics and Probability Letters* 3 (1985) 21–23.
- [69] W. Li, A. Bhalerao, R. Wilson, Analysis of retinal vasculature using a multiresolution hermite model, *IEEE Transactions on Medical Imaging* 26 (2007) 137–152.
- [70] B.S.Y. Lam, G. Yongsheng, A.W.C. Liew, General retinal vessel segmentation using regularization-based multiconcavity modeling, *IEEE Transactions on Medical Imaging* 29 (2010) 1369–1381.
- [71] H. Narasimha-Iyer, J.M. Beach, B. Khoobehi, B. Roysam, Automatic identification of retinal arteries and veins from dual-wavelength images using structural and functional features, *IEEE Transactions on Biomedical Engineering* 54 (2007) 1427–1435.
- [72] G. Xiaohong, A. Bharath, A. Stanton, A. Hughes, N. Chapman, S. Thom, A method of vessel tracking for vessel diameter measurement on retinal images. *Proceedings of International Conference on Image Processing*, 2001.
- [73] T. Zhu, Fourier cross-sectional profile for vessel detection on retinal images, *Computerized Medical Imaging and Graphics* 34 (2010) 203–212.
- [74] B. Al-Diri, A. Hunter, A ribbon of twins for extracting vessel boundaries, in: *The 3rd European Medical and Biological Engineering Conference*, Prague, Czech Republic, 2005.
- [75] B. Al-Diri, A. Hunter, D. Steel, An active contour model for segmenting and measuring retinal vessels, *IEEE Transactions on Medical Imaging* 28 (2009) 1488–1497.
- [76] A. Gooya, L. Hongen, K. Matsumiya, K. Masamune, Y. Masutani, T. Dohi, A Variational Method for Geometric Regularization of Vascular Segmentation in Medical Images, *IEEE Transactions on Image Processing* 17 (2008) 1295–1312.
- [77] L.M. Lorigo, O.D. Faugeras, W.E.L. Grimson, R. Keriven, R. Kikinis, A. Nabavi, C.F. Westin, CURVES: Curve evolution for vessel segmentation, *Medical Image Analysis* 5 (2001) 195–206.
- [78] K.W. Sum, P.Y.S. Cheung, Vessel Extraction Under Non-Uniform Illumination: A Level Set Approach, *IEEE Transactions on Biomedical Engineering* 55 (2008) 358–360.
- [79] M.M. Fraz, P. Remagnino, A. Hoppe, B. Uyyanonvara, S.A. Barman, Retinal Vessel Extraction using First-order Derivative of Gaussian and Morphological Processing, in: *7th International Symposium on Visual Computing*, Las Vegas, Nevada, USA, 2011.
- [80] A.M. López, D. Lloret, J. Serrat, J.J. Villanueva, Multilocal creaseness based on the level-set extrinsic curvature, *Computer Vision and Image Understanding* 77 (2000) 111–144.
- [81] J. Serra, *Image Analysis and Mathematical Morphology*, Academic Press, Inc, Orlando, FL, USA, 1983.
- [82] R.M. Rangayyan, *Biomedical Image Analysis*, CRC Press, Boca Raton, 2004.
- [83] M.M. Fraz, M.Y. Javed, A. Basit, Retinal Vessels Extraction Using Bitplanes. *Eight IASTED International Conference on Visualization, Imaging, and Image Processing*, Palma De Mallorca, Spain, 2008.